

## WASP-107b’s density is even lower: a case study for the physics of planetary gas envelope accretion and orbital migration

CAROLINE PIAULET,<sup>1</sup> BJÖRN BENNEKE,<sup>1</sup> RYAN A. RUBENZAHN,<sup>2</sup> ANDREW W. HOWARD,<sup>2</sup> EVE J. LEE,<sup>3</sup>  
DANIEL THORNGREN,<sup>1</sup> RUTH ANGUS,<sup>4,5</sup> MERRIN PETERSON,<sup>1</sup> JOSHUA E. SCHLIEDER,<sup>6</sup> MICHAEL WERNER,<sup>7</sup>  
LAURA KREIDBERG,<sup>8</sup> TAREQ JAOUNI,<sup>9</sup> IAN J. M. CROSSFIELD,<sup>10</sup> DAVID R. CIARDI,<sup>11</sup> ERIK A. PETIGURA,<sup>12</sup>  
JOHN LIVINGSTON,<sup>13</sup> COURTNEY D. DRESSING,<sup>14</sup> BENJAMIN J. FULTON,<sup>15</sup> CHARLES BEICHMAN,<sup>7,11</sup>  
JESSIE L. CHRISTIANSEN,<sup>11</sup> VAROUJAN GORJIAN,<sup>7</sup> KEVIN K. HARDEGREE-ULLMAN,<sup>11</sup> JESSICA KRICK,<sup>11</sup> AND  
EVAN SINUKOFF<sup>2,16</sup>

<sup>1</sup>Department of Physics, and Institute for Research on Exoplanets, Université de Montréal, Montreal, H3T 1J4, Canada

<sup>2</sup>Cahill Center for Astrophysics, California Institute of Technology, 1216 East California Boulevard, Pasadena, CA 91125, USA

<sup>3</sup>Department of Physics and McGill Space Institute, McGill University, 3550 rue University, Montreal, QC, H3A 2T8, Canada

<sup>4</sup>Department of Astrophysics, American Museum of Natural History, 200 Central Park West, Manhattan, NY, USA

<sup>5</sup>Center for Computational Astrophysics, Flatiron Institute, 162 5th Avenue, New York, NY, 10010, USA

<sup>6</sup>NASA Goddard Space Flight Center, 8800 Greenbelt Road, MD, USA

<sup>7</sup>Jet Propulsion Laboratory, California Institute of Technology, 4800 Oak Grove Drive, Pasadena, CA 91109, USA

<sup>8</sup>Max Planck Institute for Astronomy, Königstuhl 17, 69117 Heidelberg, Germany

<sup>9</sup>Department of Physics, University of Ottawa, 25 Templeton St., Ottawa, ON, K1N 6N5, Canada

<sup>10</sup>Department of Physics & Astronomy, University of Kansas, 1082 Malott, 1251 Wescoe Hall Dr., Lawrence, KS 66045, USA

<sup>11</sup>Caltech/IPAC-NASA Exoplanet Science Institute, 770 S. Wilson Ave, Pasadena, CA 91106, USA

<sup>12</sup>Department of Physics & Astronomy, University of California Los Angeles, Los Angeles, CA 90095, USA

<sup>13</sup>Department of Astronomy, University of Tokyo, 7-3-1 Hongo, Bunkyo-ku, Tokyo 113-0033, Japan

<sup>14</sup>Department of Astronomy, University of California, Berkeley, CA 94720

<sup>15</sup>NASA Exoplanet Science Institute, California Institute of Technology, 1200 East California Blvd, Pasadena, CA 91125, USA

<sup>16</sup>Institute for Astronomy, University of Hawai’i at Mānoa, Honolulu, HI 96822, USA

Submitted to ApJ

### ABSTRACT

With a mass in the Neptune regime and a radius of Jupiter, WASP-107b presents a challenge to planet formation theories. Meanwhile, the planet’s low surface gravity and the star’s brightness also make it one of the most favorable targets for atmospheric characterization. Here, we present the results of an extensive 4-year Keck/HIRES radial-velocity (RV) follow-up program of the WASP-107 system and provide a detailed study of the physics governing the accretion of its gas envelope. We reveal that WASP-107b’s mass is only 1.8 Neptune masses ( $M_b = 30.5 \pm 1.7 M_{\oplus}$ ). The resulting extraordinarily low density suggests that WASP-107b has a H/He envelope mass fraction of  $> 85\%$  unless it is substantially inflated. The corresponding core mass of  $< 4.6 M_{\oplus}$  at  $3\sigma$  is significantly lower than what is traditionally assumed to be necessary to trigger massive gas envelope accretion. We demonstrate that this large gas-to-core mass ratio most plausibly results from the onset of accretion at  $\gtrsim 1$  AU onto a low-opacity, dust-free atmosphere and subsequent migration to the present-day  $a_b = 0.0566 \pm 0.0017$  AU. Beyond WASP-107b, we also detect a second more massive planet ( $M_c \sin i = 0.36 \pm 0.04 M_J$ ) on a wide eccentric orbit ( $e_c = 0.28 \pm 0.07$ ) which may have influenced the orbital migration and spin-orbit misalignment of WASP-107b. Overall, our new RV observations and envelope accretion modeling provide crucial insights into the intriguing nature of WASP-107b and the system’s formation history. Looking ahead, WASP-107b will be a keystone planet to understand the physics of gas envelope accretion.

*Keywords:* planetary systems – planets and satellites: detection – planets and satellites: individual (WASP-107b and c) – planets and satellites: formation – planets and satellites: atmospheres

## 1. INTRODUCTION

Plentiful discoveries in exoplanetary science have revealed a great diversity of planetary systems, raising so far more new questions regarding the formation of planets than they have provided answers. The formation, evolution and orbital migration mechanisms of hot Jupiters and sub-Neptunes, for instance, which have no analogue around the sun, are challenging current theories that were originally developed solely based on Solar System observations (Lee & Chiang 2016, Dawson & Johnson 2018). Similarly, detailed investigations of exoplanets straddling the boundary between ice and gas giants, so-called “super-Neptunes” with masses intermediate between that of Neptune and Saturn, have the potential to reshape our understanding of planetary formation and migration (e.g. Lee 2019).

WASP-107b is a super-puffy super-Neptune discovered by WASP-South (Anderson et al. 2017). Transit lightcurves obtained with WASP-South and *K2*, combined with CORALIE RV measurements (Anderson et al. 2017, Dai & Winn 2017) place this planet directly at the transition between the ice and gas giants of the solar system. Its mass was estimated to be  $2.2 \pm 0.2 M_{\text{Nep}}$  or  $38 \pm 3 M_{\oplus}$ , but its radius is closest to that of Jupiter ( $0.94 R_J$ ). This first mass measurement identified WASP-107b as having one of the lowest bulk densities among all the discovered extrasolar planets. This suggests that WASP-107b is a gaseous planet with most of its mass contained within its massive envelope consisting primarily of hydrogen and helium (the most abundant gases in protoplanetary disks). A more precise and accurate measurement of the mass of this planet would provide critical physical constraints both on the core mass necessary to accrete such a large atmosphere and on the gas accretion processes at play, while being essential for accurate atmosphere characterization (Batalha et al. 2019).

WASP-107b is a challenge for planet formation as it harbors a large envelope yet currently orbits at a mere 0.06 AU from its star. WASP-107b’s core accreted over  $10 M_{\oplus}$  in gas, suggesting that it formed at several AU from the host star where the protoplanetary disk is rich in gas, ices and dust particles that can be accreted onto the rocky core. Therefore, WASP-107b has likely undergone inwards migration. Whether this migration was driven by interactions with the protoplanetary disk (disk-driven migration, e.g. Lin et al.

1996) or with other objects in the system (e.g. high-eccentricity pathway; Nagasawa et al. 2008) still remains unknown. Moreover, WASP-107b’s low mass suggests that it did not undergo the full extent of runaway gas accretion. However, the core-nucleated accretion theory (Pollack et al. 1996) predicts that planets that reach a core mass of about  $10 M_{\oplus}$  will undergo runaway gas accretion and reach a Jupiter mass within the disk’s lifetime. This leaves us with two unanswered questions: *How and where did WASP-107b form?* and *Which process prevented it from reaching a Jupiter mass?*

The large atmospheric scale height and favorable radius of this extremely low density planet make it a very exciting target for atmospheric characterization through transmission spectroscopy. It was observed with the *Hubble Space Telescope (HST)* in transit in the *WFC3/G102* and *G141* bandpasses, and the measured wavelength-dependent transit depth yielded a transmission spectrum in the  $\approx 0.9 - 1.6 \mu\text{m}$  region (Kreidberg et al. 2018, Spake et al. 2018). Spectral retrieval methods using these datasets have already unveiled peculiar features of the atmosphere of this planet. The presence of high-altitude aerosols was inferred from the muted spectroscopic signature of water (consistent with a solar abundance pattern; Kreidberg et al. 2018), and helium was detected, making WASP-107b the first exoplanet with a direct helium detection (Spake et al. 2018, Allart et al. 2019). However, all atmospheric studies so far relied on an uncertain and biased mass measurement (see Section 5.2), with direct implications on the assumed surface gravity and retrieval outcomes. Thus, a better mass determination is critical for interpreting spectroscopic observations.

Here, we present results from an extensive follow-up campaign of WASP-107 and detailed modeling of the accretion of WASP-107b’s envelope. We describe the Keck/HIRES observations in Section 2. We update the host star properties using *Gaia* DR2 and a new gyrochronological model (Section 3). The RV measurements (Section 4) allow us to provide an improved mass estimate and to detect a second planet in the system (Section 5). The new mass estimate constrains WASP-107b’s envelope fraction and allow us to propose a possible explanation for the origin of close-in exo-Neptunes like WASP-107b (Section 6).

## 2. SPECTROSCOPIC OBSERVATIONS

### 2.1. Keck/HIRES

We collected a total of 60 radial velocity measurements of WASP-107 over 56 nights between 2017 and 2020 using the High Resolution Echelle Spectrometer (HIRES; Vogt et al. 1994) on the Keck I Telescope. The observations were conducted by the California Planet Search (CPS; PI: Andrew Howard). The bulk of the observations was obtained as part of a K2-NASA key project between 2017 and early 2018. Following this program, we began re-monitoring the system in 2019 to better constrain the orbit of a possible second planet. The data were acquired using the ‘‘C2’’ decker, integrating until the exposure meter reached 60,000 counts (S/N  $\sim 100/\text{pixel}$ ,  $\sim 15$  minutes). Wavelength calibrations were done using the iodine cell (Butler et al. 1996). The HIRES data reduction followed the standard procedures of the California Planet Search described in Howard et al. (2010). Typical HIRES RV uncertainties are  $\sim 1.5$  m/s. For two of the nights, in which we obtained three measurements, we bin the data in units of 0.1 days, yielding a total of 57 HIRES RVs.

### 2.2. CORALIE

We supplement our radial velocity dataset with 31 CORALIE measurements obtained between 2011 and 2014, as reported in Anderson et al. (2017). The CORALIE measurements have a typical uncertainty of  $\sim 10$  m/s (see Table 1), 6 times larger than the typical uncertainties from HIRES, but improve our baseline. With the 31 CORALIE RVs, kindly provided to us by D. R. Anderson, our combined dataset consists of 91 RVs spanning  $\sim 3400$  days, with a 1072 day gap between the two (Figure 1). These RVs are included in the machine-readable version of Table 1.

## 3. HOST STAR PROPERTIES

The precision and accuracy of exoplanet parameters are tied to that of the ones of its host star. Here we refine the stellar parameters using our new Keck/HIRES spectra and derive a new estimate for the stellar age using gyrochronology.

### 3.1. Updated Stellar parameters

We use `isoclassify` (Huber et al. 2017a) in order to provide updated estimates for the stellar radius, mass, age and luminosity. We adopt as inputs to `isoclassify` the  $T_{\text{eff}}$  and  $[\text{Fe}/\text{H}]$  values from the Keck/HIRES spectra, constrained by the `SpecMatch-emp` tool (Yee et al. 2017). `SpecMatch-emp` provides constraints on the stellar parameters by comparing the Keck/HIRES spectra with an empirical spectral library. We use *JHK* 2MASS magnitudes, while the parallax, right-ascension, and declination are taken from *Gaia* DR2 (see Table 2).

**Table 1.** Sample radial velocities of WASP-107

Time (BJD <sub>TDB</sub> )	RV (m s <sup>-1</sup> )	$\sigma_{\text{RV}}$ (m s <sup>-1</sup> )	Instrument
2457760.081152	-1.38	1.72	HIRES
2457760.121746	4.83	1.57	HIRES
2457760.164031	7.16	1.55	HIRES
2457764.124912	-13.31	1.55	HIRES
2457765.058488	-2.94	1.50	HIRES
2457766.062488	3.33	1.51	HIRES
2457788.098712	1.62	1.72	HIRES
2457789.081827	3.72	1.71	HIRES
2457790.082269	-4.18	1.57	HIRES
2457791.002344	-16.74	1.61	HIRES
2457793.072951	-5.30	1.48	HIRES
2457794.970762	12.43	1.69	HIRES
2457802.923643	-27.41	1.46	HIRES
...	...	...	...
2455651.762169	-7.43	9.87	CORALIE
2455674.666370	-9.29	7.05	CORALIE
2455683.663183	8.62	6.93	CORALIE
2455706.521724	27.38	7.72	CORALIE
2455763.493443	8.98	7.96	CORALIE
2455963.760279	37.27	9.75	CORALIE
2455983.823533	-19.14	7.17	CORALIE
2456069.631011	-21.18	10.55	CORALIE
...	...	...	...

NOTE—A full version, including activity indicators, is available as a machine readable table in the electronic journal.

Our reported value of  $\log g$  in Table 2 was obtained using the grid-modeling method in `isoclassify` with a loose input constraint on  $\log g$  ( $4.7 \pm 0.2$ ). The constraint on  $\log g$  that we obtain from this first fit is used as an input to a second fit using the direct method.

The parameters that were derived by both the direct and grid-modeling methods (stellar radius and luminosity) are consistent within less than  $1\sigma$ . We report the radius and luminosity determined using the direct method, as in this mode the radius is not affected by the uncertainty on stellar models. The values that we quote for the stellar mass and age are the results obtained using the grid-modeling method.

The values of all parameters yielded by `isoclassify` are consistent with Anderson et al. (2017) and Močnik et al. (2017), and our mass estimate is more precise,

which we attribute to the higher precision of the  $T_{\text{eff}}$  and  $[\text{Fe}/\text{H}]$  obtained from our HIRES spectra.

The updated stellar parameters are listed in Table 2. We use the new stellar radius in order to update the radius and semi-major axis of WASP-107b; taking  $R_b/R_\star$  and  $a_b/R_\star$  from Dai & Winn (2017), we find  $R_b = 0.96 \pm 0.03R_J$  and  $a_b = 0.0566 \pm 0.0017$  AU.

### 3.2. Stellar age

The age of WASP-107 was previously estimated using several methods: an isochronal age estimate using BAGEMASS (Maxted et al. 2015a) yielded  $8.3 \pm 4.3$  Gyr – in agreement with the constraint we obtain with `isoclassify`, and a conflicting gyrochronological age of  $0.6 \pm 0.2$  Gyr (Močnik et al. 2017). This discrepancy can be explained by the failure of standard spin-down models to reproduce observations of reduced braking efficiency for late-K dwarfs relative to their F and G-type counterparts, leading them to experience a period of stalled rotation periods past  $\sim 700$  Myr (Agüeros et al. 2018, Curtis et al. 2019, 2020,b).

To resolve the discrepancy, we use a new gyrochronology model that accounts for stalled magnetic braking (Angus et al., in prep) in order to estimate the age of WASP-107. This model was calibrated by fitting a Gaussian process – a semi-parametric model that is flexible enough to capture the complex nature of stellar spin-down, to a number of asteroseismic stars and open clusters, including NGC 6811 which exhibits stalled magnetic braking (Curtis et al. 2019). We also use kinematic ages of *Kepler* field stars to calibrate the model for old K and early M dwarfs, where there is a dearth of suitable open cluster calibration stars. These kinematic ages also reflect the stalled magnetic braking behaviour seen in open clusters (Angus et al. 2020).

Using our new gyrochronology model, we infer an age of  $3.4 \pm 0.3$  Gyr for this star using the measured rotation period of  $17 \pm 1$  days (Anderson et al. 2017). The 0.3 Gyr uncertainty is the formal uncertainty that results from the uncertainty on the star’s rotation period, and does not account for uncertainty in the model. Quantifying the magnitude of the model uncertainty is beyond the scope of this paper and we adopt a 20% value of 0.7 Gyr as a more reasonable estimate of the true age uncertainty (Table 2). Importantly, we resolve the conflict between the age estimates and conclude that WASP-107 is not as young as previously suggested by gyrochronology models.

## 4. ANALYSIS

We use Keplerian model fitting and Bayesian model comparison in order to robustly infer planetary parameters and search for additional planets in the system

using the Keck/HIRES and CORALIE radial velocity observations.

### 4.1. Radial-velocity analysis

We fit the RV measurements using RadVel, an open source Python package for fitting Keplerian orbits to radial velocity datasets (Fulton et al. 2018). The posterior distributions of the parameters are sampled using the Markov Chain Monte Carlo (MCMC) affine-invariant sampler `emcee` (Foreman-Mackey et al. 2013). We fix the period  $P_b$  and time of conjunction  $T_{\text{conj},b}$  of WASP-107b to the *K2* transit ephemeris reported in Dai & Winn (2017). We use the conventional unbiased basis formed by the jump parameters  $h = \sqrt{e} \cos \omega$  and  $k = \sqrt{e} \sin \omega$  to fit for orbital eccentricities and arguments of periastron. The MCMC fitting basis is thus  $(K_b, \sqrt{e_b} \cos \omega_b, \sqrt{e_b} \sin \omega_b)$ , along with  $(P_c, T_{\text{conj},c}, K_c, \sqrt{e_c} \cos \omega_c, \sqrt{e_c} \sin \omega_c)$  for two-planet models. We introduce an offset term  $\gamma_i$  and a jitter term  $\sigma_i$  for each instrument ( $i = \{H, C\}$  for HIRES and CORALIE). These terms account respectively for different zero-points between HIRES and CORALIE and for additional noise (e.g. stellar jitter) not encapsulated by the single-measurement errors. The offset terms are computed using a linearized analytic solution. We invoke physical priors on the RV semiamplitude  $K > 0$  and eccentricity  $e \in [0, 1)$ . This brings the total of fitting parameters to 17 for a joint 2-planet fit of the HIRES and CORALIE data.

We perform a maximum-a-posteriori (MAP) fit and use the best-fit parameters to seed a MCMC that estimates the full posterior. We run the MCMC with 4 ensembles of 200 walkers each of which are allowed to burn-in until the Gelman-Rubin statistic is  $< 1.01$ , checking for convergence after 2,000 steps per walker. We then save every 5<sup>th</sup> step as a posterior sample until either 10,000 samples per walker are reached or the Gelman-Rubin statistic decreases below 1.005, at which point we consider the chains to be well-mixed. A second MAP fit is then run, starting at the median values determined by the MCMC posteriors.

We also attempted to use Gaussian process (GP) regression in order to mitigate the effect of stellar activity on the RVs by training the GP on ancillary *K2* time series, but found that adding the GP parameters to the RV fit was disfavored from a model comparison point of view (using Bayes factors; see Section 4.2) and did not improve our constraints on the planet parameters.

### 4.2. Model Comparison

We perform a total of four fits: a 1-planet and 2-planet fit to the HIRES RVs alone, and the same two fits to the

Parameter	Value	Source
<i>Identifying information</i>		
EPIC ID	228724232	
$\alpha_{J2000}$ R.A. (hh:mm:ss)	12:33:32.84	<i>Gaia</i> DR2 (Gaia Collaboration et al. 2018)
$\delta_{J2000}$ Decl. (dd:mm:ss)	-10:08:46.22	<i>Gaia</i> DR2 (Gaia Collaboration et al. 2018)
<i>Photometric properties</i>		
B (mag)	14.62±1.20	Høg et al. (2000)
V (mag)	11.47±0.20	Høg et al. (2000)
G (mag)	11.1740±0.0009	<i>Gaia</i> DR2 (Gaia Collaboration et al. 2018)
J (mag)	9.378±0.021	2MASS (Cutri et al. 2003)
H (mag)	8.777±0.026	2MASS (Cutri et al. 2003)
K (mag)	8.637±0.023	2MASS (Cutri et al. 2003)
<i>Spectroscopic and Derived properties</i>		
$\mu_\alpha$ (mas yr <sup>-1</sup> )	-96.647±0.110	<i>Gaia</i> DR2 (Gaia Collaboration et al. 2018)
$\mu_\delta$ (mas yr <sup>-1</sup> )	-9.483±0.058	<i>Gaia</i> DR2 (Gaia Collaboration et al. 2018)
Parallax (mas)	15.4175±0.0617	<i>Gaia</i> DR2 (Gaia Collaboration et al. 2018)
Distance (pc)	64.7±0.3	Bailer-Jones et al. (2018)
Spectral Type	K6	Anderson et al. (2017)
T <sub>eff</sub> (K)	4425 ± 70	This Paper (SpecMatch-emp)
[Fe/H]	+0.02 ± 0.09	This Paper (SpecMatch-emp)
log g <sub>*</sub>	4.633±0.012	This Paper (isoclassify)
M <sub>*</sub> (M <sub>⊙</sub> )	0.683 <sup>+0.017</sup> <sub>-0.016</sub>	This Paper (isoclassify)
R <sub>*</sub> (R <sub>⊙</sub> )	0.67±0.02	This Paper (isoclassify)
L <sub>*</sub> (L <sub>⊙</sub> )	0.132±0.003	This Paper (isoclassify)
P <sub>rot</sub> (days)	17±1	Anderson et al. (2017)
Age (Gyr)	8.3±4.3	Močnik et al. (2017); Isochronal (BAGEMASS)
	6.9 <sup>+3.7</sup> <sub>-3.4</sub>	This Paper; Isochronal (isoclassify)
	3.4±0.7	This Paper; Gyrochronological

**Table 2.** Stellar Parameters of WASP-107

combined HIRES and CORALIE dataset. Model comparison is performed within a robust Bayesian framework, using the Bayesian evidence and Bayes factors assuming equally probable hypotheses a-priori. A higher Bayesian evidence for a model including more free parameters indicates that the additional model complexity is granted by the quality of the data. Hence, the model with the highest Bayesian evidence is favored. For each model of the RVs, we approximate the Bayesian evidence using the estimator presented in Perrakis et al. (2014) (as in e.g. Cloutier et al. 2019). This method consists in using the product of marginalized posterior distributions of “blocks” of parameters (obtained after a rearrangement of the parameters in MCMC chains) as an importance sampler in the evidence estimation. Nelson et al. (2020) found that this estimator obtains results in good agreement with more computationally-intensive methods (e.g., Nested Sampling) while requiring no additional sampling of the parameter space. On the other hand, they found that non-bayesian methods such as Bayesian Information Criteria (BIC) that are

based on simplifying assumptions such as an infinitely narrow posterior only poorly approximate the Bayesian evidence and can lead to false-negatives in planet detections using RVs. In this work, we use the implementation of this estimator in the `bayev` package, publicly available on GitHub<sup>1</sup>. Each block consists of only one of the fitted parameters. The importance sampler is obtained after a random rearrangement of the parameters and we use kernel density estimations of each marginalized posterior distribution of samples. For each model, we perform 1,000 such rearrangements, calculating the Bayesian evidence for each and quote the median from these values.

## 5. RESULTS

### 5.1. Detection of a long-period companion

The HIRES data exhibit a significant long-period trend on top of the signal from WASP-107b due to

<sup>1</sup> <https://github.com/exord/bayev>

**Table 3.** Keplerian model comparison. The Bayes factors are reported relative to the single-planet model. In both cases, the 2-planet model is favored.

Model	$\ln p(D \mathcal{M}_i)$	$\frac{p(D \mathcal{M}_2)}{p(D \mathcal{M}_1)}$	“Sigma” <sup>a</sup>
<b>HIRES</b>			
1-Planet	-174.3	–	–
2-Planet	-156.6	$4.9 \times 10^7$	$6.3\sigma$
<b>HIRES + CORALIE</b>			
1-Planet	-290.1	–	–
2-Planet	-156.4	$1.2 \times 10^{58}$	$16.5\sigma$

<sup>a</sup>The correspondence between the Bayes factors and the “sigma” significance in a frequentist framework is calculated using p-values, as presented in [Trotta \(2008\)](#).

the presence of a second planet in a long period orbit (Figure 1). Our Bayesian model comparison based on the HIRES data alone favors the two-planet model at  $4.9 \times 10^7$  to 1 in the Bayes factor (equivalently  $6.3\sigma$ ; Table 5.1). The evidence for the existence of this second planet, WASP-107c, is further strengthened by including the previously obtained CORALIE dataset in the radial velocity analysis (see Table 5.1). Overall, the CORALIE dataset increases the baseline by a factor of  $\sim 3$ , allowing us to rule out a 1-planet model in favor of a two-planet Keplerian solution, with a Bayes factor of  $1.2 \times 10^{58}$  to 1 (or a  $16.5\sigma$  significance). The best-fit two-planet model to the combined dataset is shown in Figure 1. In what follows, we will report constraints on the orbital parameters based on the two-planet model and the combined dataset.

### 5.2. Mass and Orbital Constraints

MCMC parameter estimates and uncertainties are displayed in Table 4 along with derived planet parameters. The corresponding joint and marginalized posterior distributions are shown in Figure 2. We find a revised mass for WASP-107b of  $M_b = 30.5 \pm 1.7 M_\oplus$  and an eccentricity of  $e_b = 0.06 \pm 0.04$ . This lower mass associated with a Jupiter radius makes WASP-107b an outlier in the mass-radius diagram (Figure 3). Combined with the transit measurement for the radius, we find the bulk density of WASP-107b to be  $\rho_b = 0.134^{+0.015}_{-0.013} \text{ g cm}^{-3}$ , even lower than the previous estimate of  $0.19 \pm 0.03 \text{ g cm}^{-3}$  ([Anderson et al. 2017](#)).

The HIRES and CORALIE datasets combined constrain the RV semi-amplitude of the outer companion to  $K_c = 9.6^{+1.1}_{-1.0} \text{ m s}^{-1}$ , corresponding to a mass of

**Table 4.** MCMC Posteriors for the WASP-107 System

Parameter	Unit	Credible Interval
<b>Orbital Parameters</b>		
$P_b$	days	$\equiv 5.7214742$
$T_{\text{conj},b}$	BJD <sub>TDB</sub>	$\equiv 2457584.329897$
$e_b$		$0.06 \pm 0.04$
$\omega_b$	deg	$40^{+40}_{-60}$
$K_b$	$\text{m s}^{-1}$	$14.1 \pm 0.8$
$P_c$	days	$1088^{+15}_{-16}$
	yrs	$2.98 \pm 0.04$
$T_{\text{conj},c}$	BJD <sub>TDB</sub>	$2458520^{+60}_{-70}$
$e_c$		$0.28 \pm 0.07$
$\omega_c$	deg	$-120^{+30}_{-20}$
$K_c$	$\text{m s}^{-1}$	$9.6^{+1.1}_{-1.0}$
<b>Derived Parameters</b>		
$M_b$	$M_\oplus$	$30.5 \pm 1.7$
	$M_J$	$0.096 \pm 0.005$
$\rho_b$	$\text{g cm}^{-3}$	$0.134^{+0.015}_{-0.013}$
$M_c \sin i$	$M_\oplus$	$115 \pm 13$
	$M_J$	$0.36 \pm 0.04$
$S_c^a$	mas	$26^{+8}_{-5}$
<b>Global Parameters</b>		
$\gamma_H^b$	$\text{m s}^{-1}$	$\equiv 1.52001$
$\gamma_C^b$	$\text{m s}^{-1}$	$\equiv 3.55333$
$\sigma_H$	$\text{m s}^{-1}$	$3.9^{+0.5}_{-0.4}$
$\sigma_C$	$\text{m s}^{-1}$	$5.5^{+2.8}_{-2.9}$

<sup>a</sup>Sky-projected angular separation

<sup>b</sup>Reference epoch for  $\gamma$ : 2457934.793533

$M_c \sin i = 0.36 \pm 0.04 M_J$ . The orbital period of the outer planet ( $2.98 \pm 0.04$  years) and its eccentricity ( $e_c = 0.28 \pm 0.07$ ) are well constrained thanks to the detection of two steep rises in RV throughout the HIRES observing campaign. Continued monitoring of this system will enable further refinements of the orbit of this outer planetary companion.

### 5.3. An even lower mass for WASP-107b

Our measurement of WASP-107b’s mass of  $30.5 \pm 1.7 M_\oplus$  is substantially lower than the inferred  $38 \pm 3 M_\oplus$  reported by [Anderson et al. \(2017\)](#) from the analysis of the CORALIE dataset. We argue that this discrepancy

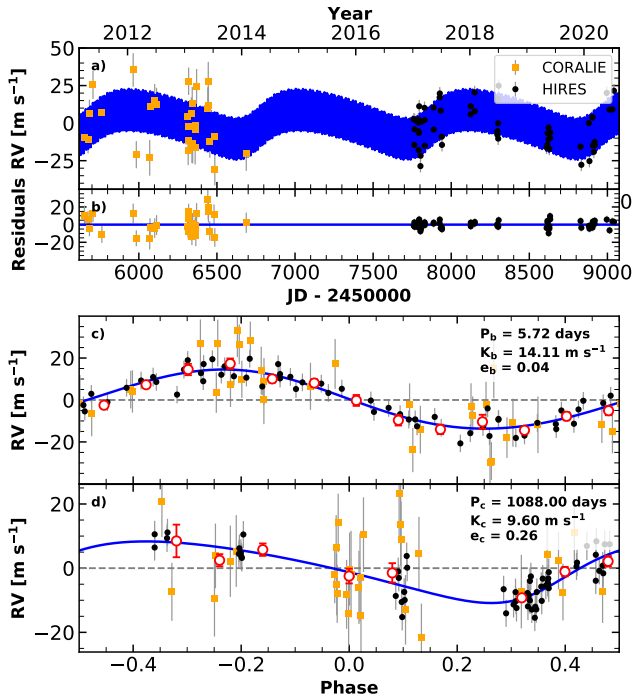


**Figure 1.** Maximum-likelihood two-planet Keplerian orbital model for WASP-107. **a)** The best-fitting model is plotted while the annotated orbital parameters are the corresponding MAP fit parameters. The blue line is the best fit two-planet model. We add in quadrature the RV jitter terms listed in Table 4 with the measurement uncertainties for all RVs. **b)** Residuals to the best fit two-planet model. **c)** RVs phase-folded to the ephemeris of planet b. The Keplerian orbital model for the other planet has been subtracted. The small point colors and symbols are the same as in panel a. Red circles are the same velocities binned in units of 0.08 in orbital phase. The phase-folded model for planet b is shown as the blue line, with the corresponding best-fit keplerian model parameters quoted. **d)** The same for planet c.

can be explained as arising from the improved precision of the HIRES RV measurements.

Our new mass estimate for WASP-107b is 20% lower than the previously-published one, and lies  $\approx 2.2\sigma$  away from it. For a fitted semi-amplitude  $K$  to a time series of  $N_{obs}$  radial velocities having a typical measurement uncertainty  $\sigma$ ,  $K$  will be biased towards a higher value than the true one if  $K/\sigma$  or  $N_{obs}$  is small (Shen & Turner 2008). Thus, with  $N_{obs} = 31$  and  $K/\sigma < 2$ , the CORALIE dataset is expected to suffer from this bias more than the HIRES measurements, where  $N_{obs} = 60$  and  $K/\sigma \approx 11$ . Moreover, Anderson et al. (2017) fixed the eccentricity to zero (yielding smaller uncertainties on  $K$ ) and used a larger stellar mass compared to our new determination, which further contributed to a larger estimated planet mass.

#### 5.4. Gas-to-core mass ratio

Our new mass measurement indicates that WASP-107b has an extraordinarily low density. We infer the gas-to-core mass ratio of WASP-107b by comparing our measurements to model predictions for various envelope mass fractions (Figure 3). We generate grids of thermal evolution models and predict 10-mbar radii for planets with varying incident fluxes  $S_{inc}$ , masses  $M_p$ , ages and fractions  $f_{env}$  [%] of their masses contained in the H/He envelopes surrounding their cores. Previously available model grids in the literature (e.g. Lopez & Fortney 2014) do not extend all the way to the mass and radius of WASP-107b and could not yet make use of the latest equation of state for hydrogen.

We compute the thermal evolution models as described in Thorngren et al. (2016). The atmosphere models are interpolated from the Fortney et al. (2007) solar-metallicity grids and serve as a boundary condition to interior structure models. We use updated equations of state (EOS) for the solar-ratio H/He gas (Chabrier et al. 2019) and choose the Thompson (1990) EOS for metals. Since the composition of the core of WASP-107b is unknown, we marginalize over the uncertainty on the fraction of water within its core by producing two grids for planets with either an Earth-like core (67.5% rock, 32.5% Fe by mass) or a pure water composition. Therefore, the true envelope mass fraction of the planet should lie in the range cornered by the two derived envelope mass fractions: the same planet radius and mass will yield a larger inferred H/He mass fraction if the core composition is rocky than if it is water-rich. The two-layer models include no mixing from the core into the envelope and in the pure-water core case, we include convection in the water component. Our grids span the range 10 to  $10^5 S_{\oplus}$  for incident flux, 15 to 40  $M_{\oplus}$  for planet mass, 0.1 to 14 Gyr in terms of system age and H/He envelope mass fractions of 0.01 to 100%. The curves of constant  $f_{env}$  in the mass-radius diagram computed using the median parameters for WASP-107b already suggest an extremely high envelope mass (Figure 3).

More quantitatively, we solve the inverse problem of inferring an envelope mass fraction from the planet’s incident flux, mass, age and radius using the `smint` (Structure Model INterpolator) interpolation and envelope mass fraction fitting package, which we made publicly-available on GitHub<sup>2</sup>. From any set of parameters ( $S_{inc}$ ,  $M_p$ , age,  $f_{env}$ ), `smint` returns a planet radius by performing linear interpolation over a grid of  $f_{env}$ ,

<sup>2</sup> <https://github.com/cpiaulet/smint>

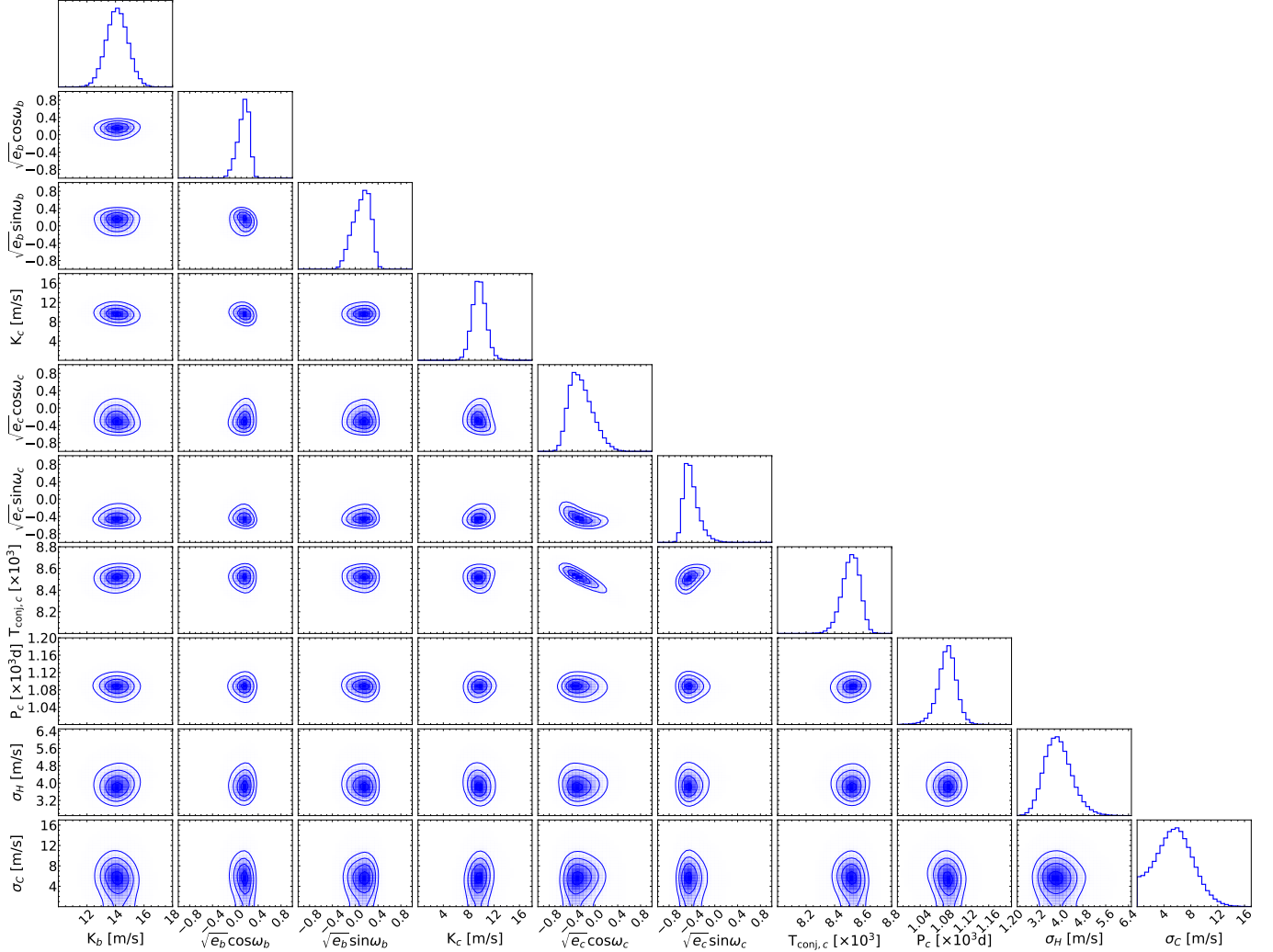


**Figure 2.** Joint and marginalized posterior distributions from the two-planet fit to the combined HIRES+CORALIE dataset.

$\log_{10} M_p/M_{\oplus}$ , system age and  $\log_{10} S_{inc}/S_{\oplus}$  set up using one of our model grids. We run a MCMC that fits for the combination of  $(S_{inc}, M_p, \text{age}, f_{env})$  which best matches the observed planet radius. We adopt gaussian priors on  $S_{inc}$ ,  $M_p$  and the system’s age informed by the parameters derived from the RV fits and the gyrochronology model. We use a uniform prior on the planet’s envelope mass fraction over the entire range spanned by the grid. Each of the 100 chains is run for 10,000 steps, 60% of which are discarded as burn-in. The autocorrelation times of the fitted parameters are all  $\leq 52$  steps (less than 15% of the length of the chains past the burn-in phase), securing that our chains are converged and sample well the posterior PDFs. We perform two fits using the grids for the Earth-like and pure H<sub>2</sub>O core compositions.

We infer upper limits on the core mass of 3.7 and 4.6  $M_{\oplus}$  at  $3\sigma$  (lower masses are excluded with 99.7% confidence) for the Earth-like and pure H<sub>2</sub>O core re-

spectively, corresponding to envelope mass fractions of 88% and 85% for a solar metallicity envelope (Figure 4). As expected, we find a correlation between the system’s age and the inferred envelope mass fraction due to the contraction and cooling of the planet as it ages. The inferred core mass is much smaller than traditionally assumed to be required for the triggering of runaway gas accretion. Interestingly, the small core still must have been able to accrete almost 30  $M_{\oplus}$  in gas from the surrounding nebula once it had coagulated.

Our estimate also serves as a conservative lower limit on the initial accreted envelope mass, given that planets undergo atmospheric loss throughout their existence (e.g. Owen & Wu 2013, Owen, & Wu 2016). In fact, the puffiness and close-in orbital distance of WASP-107b places it at the cusp of the sub-Jovian desert (e.g. Mazeh et al. 2016, Owen & Lai 2018). In particular, we find that assuming a zero Bond albedo, WASP-107b’s core would need to be more massive than 4.1  $M_{\oplus}$  ( $1\sigma$  upper



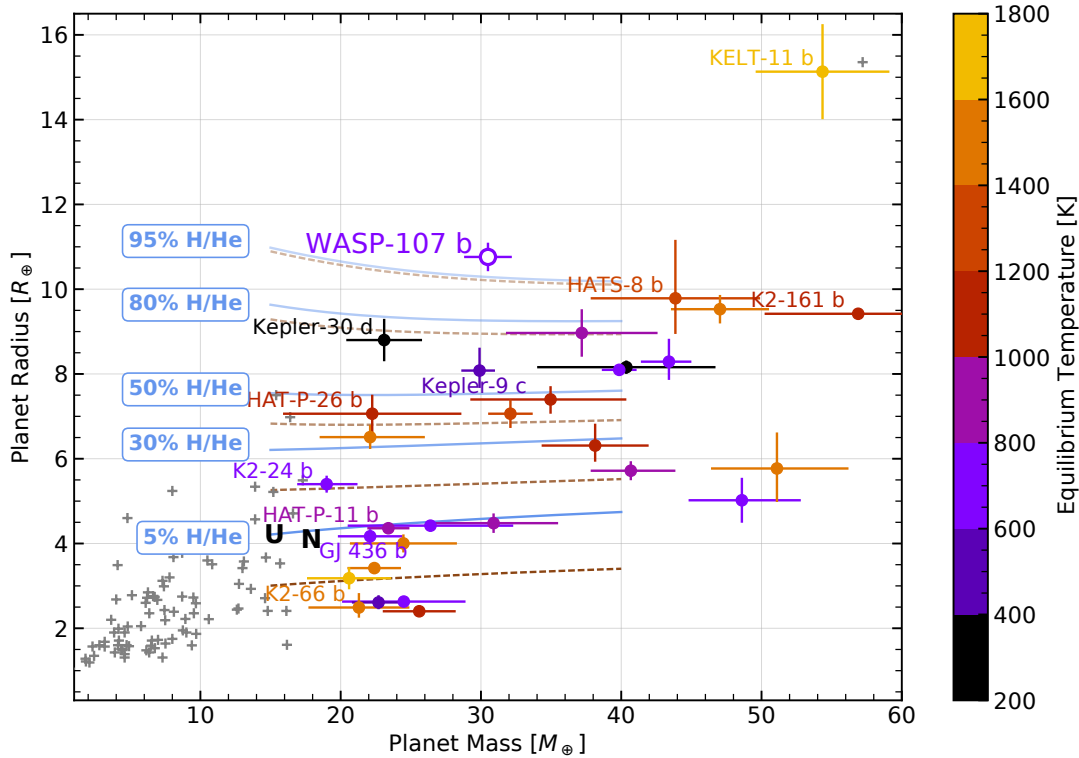


**Figure 3.** Mass-radius diagram of the detected exoplanets with a mass and radius measured with 30% or higher precision, zoomed-in on super-Neptunes having masses between 20 and 60  $M_{\oplus}$  (colored by equilibrium temperature). The positions of Uranus and Neptune are indicated by black letters. The solid blue and dashed saddlebrown curves correspond to various envelope mass fractions from the grid of solar-metallicity envelopes atop pure  $H_2O$  or Earth-like cores respectively, interpolated to match an age of 3.4 Gyr and the incident flux corresponding to WASP-107b. If no inflation mechanism is considered, we obtain a  $3\sigma$  lower limit on the envelope mass fraction of 85%, which corresponds to a core mass of only 4.6  $M_{\oplus}$ . The larger KELT-11b may be inflated due to its high equilibrium temperature (Pepper et al. 2017).

limit accounting for the uncertainties on the stellar and orbital parameters) for the atmosphere to survive photoevaporation at its present orbital location (Ginzburg et al. 2016). This limit is higher than our above-mentioned estimates of the core mass, suggesting that WASP-107b migrated to its present orbital location only recently (see Section 6.5).

The large H/He mass fraction of WASP-107b strikingly contrasts with those of the ice giants of our Solar System (5–15% H/He for both Uranus and Neptune, Podolak & Marley 1991, Guillot 2005). Instead, WASP-107b’s structure most closely resembles those of Jupiter and Saturn, composed of more than 90% H/He by mass. WASP-107b is an extreme case even among the vastly diverse exoplanet interiors illustrated by the wide span in radius of the super-Neptunes, which highlights the great diversity of formation pathways within this population. WASP-107b, with its Jupiter-like composition, resembles K2-161b and Kelt-11 b that have large envelope mass fractions ( $> 75\%$ ) associated with their low densities (Brahm et al. 2019, Pepper et al. 2017). Meanwhile, thermal evolution models predict for instance a

Neptune-like structure for the 23  $M_{\oplus}$  planet HAT-P-11b, with about 15% H/He by mass (Petigura et al. 2017).

## 6. IMPLICATIONS FOR PLANET FORMATION

In light of the results from our radial-velocity analysis, we find that WASP-107b likely has an extremely large gas-to-core mass ratio (GCR; Section 5.4). This makes it one of the puffiest Neptune-mass planets known to date and raises two important questions: *How could a core of  $< 4.6 M_{\oplus}$  accrete such a massive envelope?* and *How was its transformation into a Jupiter-mass gas giant thwarted?* As such an extreme case, WASP-107b motivates a detailed investigation of the physics of gas accretion and orbital migration at play.

### 6.1. Planet formation scenarios

According to the core-nucleated accretion theory (Perri & Cameron 1974, Mizuno 1980, Pollack et al. 1996), which stands as the “standard model” for planet formation, a planetary core will first assemble from the solids present in its neighborhood within the protoplan-

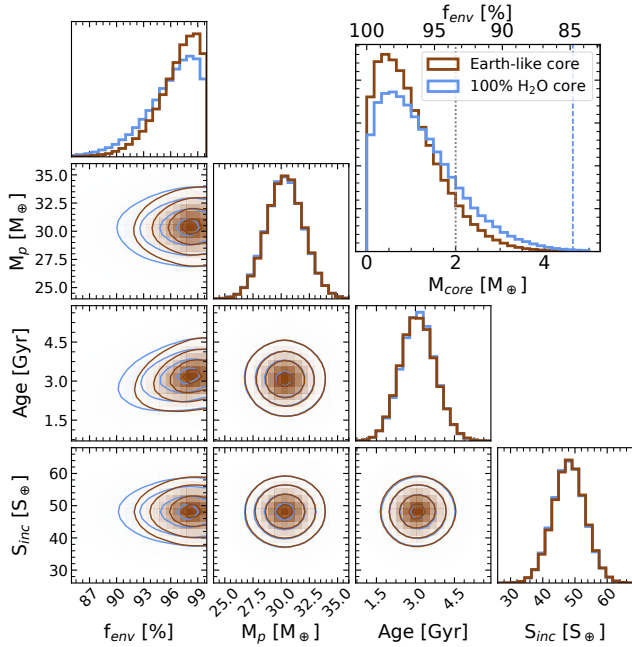


**Figure 4.** Constraints on the envelope mass fraction and core mass of WASP-107b from our models assuming either an Earth-like or a pure-water core composition. The joint and marginalized posterior distributions for a  $1 \times$  solar metallicity envelope are shown in blue and gray respectively, along with the corresponding distribution of core masses. The dotted gray line corresponds to a core mass of  $2 M_{\oplus}$  which we use in our envelope accretion simulations (Section 6). We place a  $3\sigma$  upper limit of  $4.6 M_{\oplus}$  on the mass of the pure water core (dashed blue line).

etary disk. Past this phase of solid accretion, a second phase will start, dominated by gas accretion. The rate of envelope accretion is governed by cooling of the gas (Lee & Chiang 2015, Ginzburg et al. 2016) and by local and global hydrodynamic flows (Tanigawa & Tanaka 2016). Lee (2019) demonstrated that the observed distribution of GCRs can effectively be reproduced if all these mechanisms are taken into account. For core masses below  $\approx 20 M_{\oplus}$ , the cooling timescale remains the longest until the runaway is triggered (Figure 2 of Lee 2019) beyond which the rapid dispersal of background disk limits the delivery of gas onto planets. We note here that this rapid dispersal is valid only within  $\sim 1$  AU where the photoevaporative wind is launched, carving out a gap disconnecting the inner disk from the outer disk (Owen et al. 2011).

To reproduce the inferred GCR of WASP-107b, we need to identify the gas accretion scenario in which the runaway growth begins but is curbed prematurely within the typical disk lifetime  $\sim 1$ – $10$  Myrs (e.g., Haisch et al. 2001, Mamajek 2009, Pfalzner et al. 2014, Alexander et al. 2014). We explore two potential pathways,

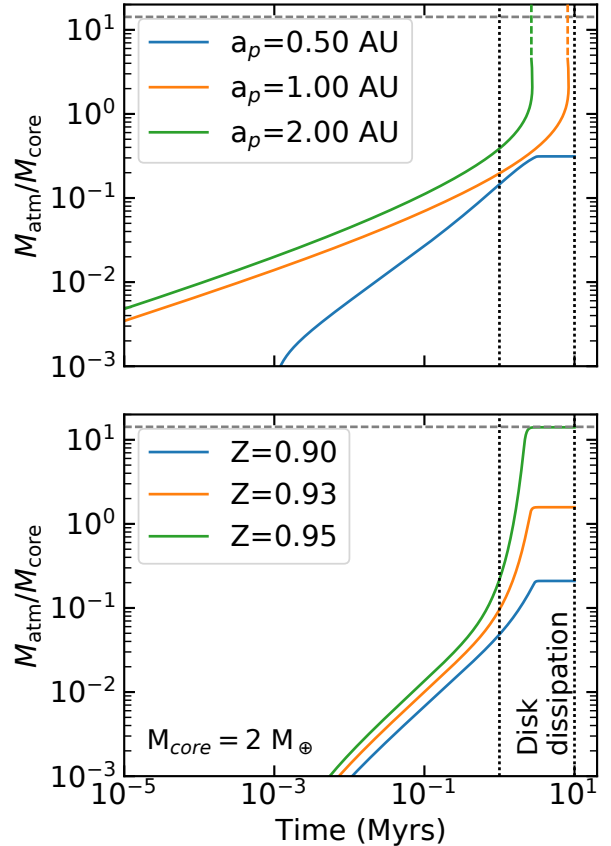


**Figure 5.** Potential formation pathways of WASP-107b for a  $2 M_{\oplus}$  core. Two different modes of gas accretion are explored: dust-free, solar metallicity gas (top panel) and dusty, metal-enriched gas (bottom panel). The orbital distance is freely varied in dust-free calculation while the dusty calculation was performed in situ (0.05 AU). The GCR that is consistent with the measured mass of WASP-107b for a  $2 M_{\oplus}$  core (dashed gray line) is above unity, well beyond the triggering of runaway, super-exponential growth. This simulation highlights the plausible parameter space that can match the target GCR within the typical disk gas dissipation time (delimited by the vertical dotted lines). Inside 1 AU, runaway gas accretion can be quenched by the rapid disk gas dispersal before the planet blows up into a gas giant.

motivated by the results of Lee & Chiang (2015). First, we consider dust-free accretion at distances beyond the present-day orbit of WASP-107b. Second, we consider in-situ (0.05 AU) accretion of dusty, metal-enriched gas.

## 6.2. Dust-free accretion with solar metallicity

As dust grains coagulate and sediment, they no longer contribute to the atmospheric opacity (e.g., Ormel 2014, Mordasini 2014, Piso et al. 2015). The upper radiative layer becomes largely isothermal so that the envelope becomes colder at larger stellocentric distances. As the internal modes of gaseous molecules gradually freeze

out, the opacity drops and the envelope cools faster and therefore grows faster. Dust-free accretion beyond  $\sim 1$  AU was invoked as a way to explain Kepler-51b, a super-puff of a  $\sim 2 M_{\oplus}$  core that accreted a  $\sim 30\%$  by mass envelope (Lee & Chiang 2016).

For WASP-107b, we adopt the procedure of Lee (2019)—where at each timestep, the rate of gas accretion is set by the minimum between cooling, local hydrodynamic, and global disk accretion—but replace the cooling calculation to that of dust-free accretion. One-dimensional structure equations are solved numerically following Lee et al. (2014), corrected for the decrease in the bound radius by three-dimensional advective flows (e.g., Lambrechts & Lega 2017). We confirm that the updated numerical solutions computed at a few orbital distances agree well with the analytic scaling relationship derived by Lee & Chiang (2015), and search for the range of potential formation locations by scaling with respect to the fiducial numerical calculation at 2 AU (see top row of Figure 5). For a core that weighs  $2 M_{\oplus}$ , dust-free accretion should have occurred at  $\gtrsim 1$  AU for the runaway to be launched.

### 6.3. Dusty accretion with supersolar metallicity

Are there ways to form WASP-107b in-situ? It appears impossible for solar metallicity gas but the rate of accretion can be boosted in highly metal-enriched environments. While this may be counter-intuitive, as higher opacity would slow down the cooling of gas, this impediment by opacity endures only up to  $Z \sim 0.2$  (10 times the solar value). Beyond this point, the mean molecular weight of the envelope becomes so high that it becomes more prone to gravitational collapse requiring more vigorous accretion in order to maintain hydrostatic equilibrium. This boost in accretion rate applies equally to dust-free and dusty accretion. Since dusty accretion is generally slower than dust-free accretion, we elect to show the former to delineate all the possible limiting cases.

We proceed the same way as in the calculation for dust-free accretion and follow the procedure of Lee (2019), accounting for the effect of metallicity in the rate of cooling, which can be written as

$$\frac{M_{\text{atm}}}{M_{\text{core}}} \sim 0.09 \left( \frac{\Sigma_{\text{gas}}}{13 \text{ g cm}^{-3}} \right)^{0.12} \left( \frac{M_{\text{core}}}{20 M_{\oplus}} \right)^{1.7} \left( \frac{t}{0.1 \text{ Myrs}} \right)^{0.4} \times \left( \frac{0.02}{Z} \right) \left( \frac{\mu}{2.37} \right)^{3.4} \text{Exp} \left( \frac{t}{t_{\text{run}}} \right) \quad (1)$$

where  $\Sigma_{\text{gas}}$  is the disk gas surface density evaluated at the position of the core and at time  $t$ ,<sup>3</sup>  $\mu$  is the mean molecular weight, and  $t_{\text{run}}$  is the runaway timescale determined numerically as the time at which  $M_{\text{atm}}/M_{\text{core}}$  reaches 0.5:

$$t_{\text{run}} \sim 2.24 \text{ Myrs} \left( \frac{20 M_{\oplus}}{M_{\text{core}}} \right)^{4.2} \left( \frac{Z}{0.02} \right) \left( \frac{2.37}{\mu} \right)^{8.5}. \quad (2)$$

Both  $Z$  and  $\mu$  are evaluated at the radiative-convective boundary, assuming  $Z$  is uniform throughout the planetary envelope.

The required metallicity enhancement is severe, due by the need to trigger the runaway prior to disk dissipation and reach the observed GCR (see bottom row of Figure 5). We find that the required metallicity is  $Z \gtrsim 0.95$ , or approximately 48 times the solar value by mass.

### 6.4. Constraints from structure evolution models

We use the same type of interior structure models as in Section 5.4 in order to constrain the range of metallicities allowed by the mass and radius of WASP-107b. The planet is modeled as a well-mixed, fully-convective envelope with a radiative atmosphere and we assume a 50-50 mixture of rock and ice for metals. We do not include a core to get a conservative (high) upper limit on the envelope metallicity (see Thorngren & Fortney 2019). Our models are sensitive to the assumed age of the system, as the planet cools and contracts over time. We set the prior on the system age to a normal distribution corresponding to the gyrochronological age ( $3.4 \pm 0.7$  Gyr; see Table 2).

We fit for the metal mass fraction using MCMC with 6 chains in parallel. In each chain, we burn in for 10,000 steps and then record every 10th step until we have amassed 100,000 samples. We infer a  $3\sigma$  upper limit of  $Z \lesssim 0.25$  on the envelope’s metal mass as higher metallicities would result in smaller radii. Interestingly, our constraint on the metallicity ( $< 12.5$  times the solar value by mass at  $3\sigma$ ) is in agreement with the metallicity constraint retrieved from the spectroscopic characterization of the  $12.6 M_{\oplus}$  sub-Neptune GJ 3470b (Benneke et al. 2019) and suggests that the two planets may have had similar formation processes.

The  $3\sigma$  upper limit of 0.25 on the envelope metallicity is 3.8 times smaller than required by the dusty

<sup>3</sup> The disk is evolved according to steady-state viscous dissipation (Lynden-Bell & Pringle 1974, Hartmann et al. 1998) up to 0.7 Myrs. Beyond that, the inner disk detaches from the outer disk and viscously drifts in over the dissipation timescale evaluated at its outer edge (Owen et al. 2011).

gas accretion models and effectively rules out the high-metallicity accretion scenario: the planet could not be this puffy to this day if such large amounts of metals were present in its atmosphere. We highlight the fact that the rate of dusty accretion is only weakly dependent on orbital distance, under the assumption that the dust-to-gas mass ratio is spatially constant within the disk. Our constraints on the envelope metallicity therefore rule out the dusty accretion scenario in disks with uniform dust-to-gas mass ratio. Furthermore, as mentioned above (Section 5.4), the observationally inferred GCR only provides a lower limit on the amount of gas accreted by the core, as mass-loss powered by stellar irradiation and the planet’s leftover heat from formation can pare down the envelope mass fraction and is believed to sculpt the radius distribution of small planets (Owen & Wu 2017, Ginzburg et al. 2018, Gupta & Schlichting 2020). Reaching a higher GCR at formation would necessitate an even higher metallicity.

This leaves dust-free accretion as the only plausible formation scenario for WASP-107b’s massive envelope. With over 85% of its mass contained in its H/He envelope, WASP-107b effectively provides evidence for the possibility of a  $< 4.6 M_{\oplus}$  core accreting extensive amounts of primordial gas.

### 6.5. Dynamical consideration

Assuming that WASP-107b indeed formed as a dust-free world at  $\gtrsim 1$  AU, it must have undergone inward migration, whether through the underlying disk in early, gas-rich environment or through perturbation by neighboring planets in late, gas-poor or gas-empty environment. We propose that the migration of WASP-107b happened early such that it went close to experiencing the full extent of runaway gas accretion before it was deprived from its supply of gas.

The fact that WASP-107b accreted copious amount of envelope suggests that it assembled early, beyond  $\sim 1$  AU. After its assembly, the planet is expected to undergo inward Type I migration (Lin et al. 1996, Papaloizou et al. 2007)– this has been proposed as the formation channel of super-puffs explaining why they are frequently observed as parts of resonant chains (Lee & Chiang 2016). Alternatively, or additionally, WASP-107b could have arrived at its present orbit through planet-planet scattering involving WASP-107c: this scenario would have the advantage of explaining the eccentricity of planet c. Still, we note that it is uncertain whether the runaway accretion can be stopped at the right time to produce WASP-107b beyond 1 AU which may suggest that WASP-107b began its inward transport just at the right time as it reached its envelope mass fraction of  $>85\%$ .

Although our constraints on the eccentricity of WASP-107b are consistent with a circular orbit at  $2\sigma$ , we find that it could have a moderate eccentricity. The timescale of tidal circularization ( $\tau_{circ} = e/\dot{e}$ ) for WASP-107b is  $\sim 66$  Myrs, much shorter than the estimated age of the system.<sup>4</sup> Any remaining eccentricity of the inner planet resulting from dynamical interactions will therefore be quickly dampened by tidal interactions with its host star. Given this short circularization timescale, a present-day eccentricity of 0.06 (median from the RV fit; see Table 4) would imply recent dynamical interactions that excited the eccentricity to high values. In particular, we demonstrate using our constraints on the WASP-107b’s orbit that tidal interactions alone could have brought the planet from  $\gtrsim 0.10$  AU to its current orbital location over less than 1 Gyr (Figure 7).

Using the occurrence of spot-crossing anomalies during planetary transits, WASP-107b was inferred to feature a high spin-orbit misalignment (40–140 degrees; Močnik et al. 2017, Dai & Winn 2017, Rubenzahl et al., submitted). Such high obliquity is often considered as a sign of dynamic upheaval and could be attributed to nodal precession as was proposed for HAT-P-11b (Yee et al. 2018). Alternatively, WASP-107b is sufficiently small in mass and sufficiently far away from the star that its natal disk could have been driven to substantial spin-orbit misalignment with respect to the central star. For a star-disk system with an outer planet that is misaligned with the disk, secular resonance between the disk’s precession around this planet and the star’s precession around the disk can drive a large star-disk misalignment (e.g., Batygin & Adams 2013, Lai 2014, Zanazzi & Lai 2018). This resonance is suppressed for rapidly rotating stars in the presence of a close-in massive inner planet (i.e., star’s precession around the inner planet is faster than the disk’s precession around the outer planet). We confirm that for WASP-107 system, star-disk misalignment by secular resonance is possible as long as WASP-107b is beyond  $\sim 0.02$  AU, which it is (equation (70) of Zanazzi & Lai (2018)). Another scenario that could account not only for the spin-orbit misalignment but also for WASP-107b’s moderate eccentricity is that of a resonance initiated during the dispersal of an otherwise coplanar protoplanetary disk (Petrovich et al. 2020). In this case, one would expect a large mutual inclination between planets b and c.

<sup>4</sup> The circularization time is evaluated using Equation (2) of Jackson et al. (2009) using the values of  $Q_p$  and  $k_{2p}$  for Jupiter from Lainey et al. (2009), with  $Q'_p = Q_p/k_{2p}$  (Goldreich & Soter 1966), and  $Q'_*$  from Equations (1) and (2) of Penev et al. (2018).

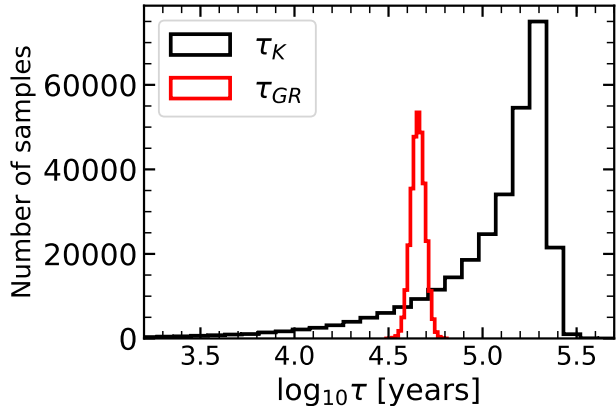


**Figure 6.** Distributions of the timescales of Kozai cycles ( $\tau_K$ ) and GR apsidal precession ( $\tau_{GR}$ ). In most cases,  $\tau_K \gg \tau_{GR}$  and Kozai cycles would be efficiently suppressed.

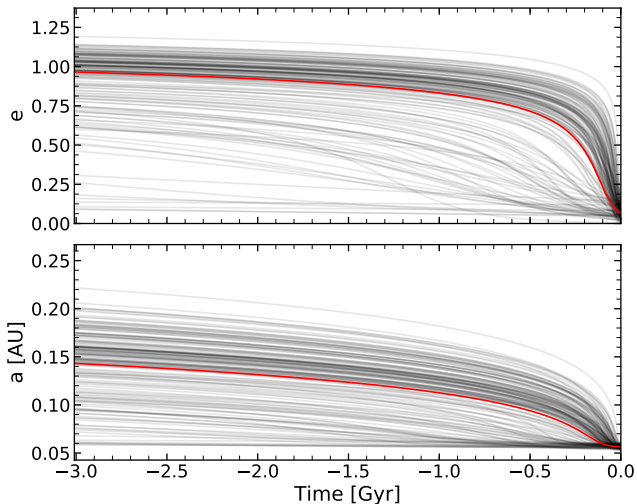


**Figure 7.** Orbital evolution of WASP-107b (eccentricity in the top panel, semi-major axis in the bottom panel) over the past 3 Gyr, under the influence of tidal interactions from its host star alone (Jackson et al. 2009). The black curves are the results of 200 simulations of the orbital evolution, randomly varying relevant system parameters using their mean and  $1\sigma$  uncertainties. The red curve corresponds to a simulation using the median present-day values of each parameter.

Alternatively, we examined whether Kozai-Lidov cycles induced by the presence of planet c could explain the high obliquity of WASP-107b and its moderate eccentricity. We calculate the Kozai timescale (Kiseleva et al. 1998) using our posterior chains and considering a random inclination for planet c. Comparing it to the period of general relativistic (GR) apsidal precession (see Figure 6), we find that the Kozai cycles are likely suppressed by GR precession, with  $\tau_K \gg \tau_{GR}$ .

### 6.6. Tidal Inflation

The above-mentioned scenario relies on the assumption that our two-layer models represent accurate end-cases for the planetary structure. In this subsection, we consider the possibility that WASP-107b is instead a sub-Neptune with an inflated radius.

The amount of tides raised on a planet and their dissipation can increase dramatically for planets on eccentric, inclined orbits. In particular, it was suggested that WASP-107b could be a puffed-up sub-Neptune with an envelope mass fraction as low as  $\sim 10\%$  assuming an obliquity of  $\sim 60^\circ$ , a tidal quality factor of the planet  $Q'_p \sim 10^5$  and an eccentricity of  $\sim 0.13$  (approximately  $2\sigma$  higher than the limit we derive from our RV analysis; Millholland et al. 2020).

Furthermore, while we considered above the possibility that the eccentricity of WASP-107b’s orbit is associated with recent dynamical interactions, it can also be explained by a large tidal quality factor for the planet. We estimate that  $Q'_p \gtrsim 5 \times 10^6$  is required to maintain non-zero eccentricity over the system’s age against tidal circularization. Using this  $Q'_p$  and the updated eccentricity  $\sim 0.06$ , we expect significantly less inflation by tides with a dissipation rate of  $\sim 7 \times 10^{25}$  ergs  $s^{-1}$  (approximately one order of magnitude less than the estimates of Millholland et al. 2020). Without running an evolutionary model, we cannot determine the expected envelope mass fraction in the presence of tidal dissipation but we estimate that it would be greater than  $\sim 30\text{--}40\%$  based on Figure 6 of Millholland et al. (2020), which is large enough to have initial radii of  $\gtrsim 4R_\oplus$  (i.e., a sub-Saturn). In this case, WASP-107b would have a core that weighs  $18\text{--}21M_\oplus$ . We find that in this case, its formation can be reconciled with in-situ dusty accretion with  $Z \sim 0.1\text{--}0.3$ .

While the order of magnitude of the tidal quality factor is unconstrained observationally for this planet and higher values would lead to a lesser impact of tides on the planetary radius, tidal inflation could provide an alternative explanation for the low measured density of WASP-107b.

## 7. CONCLUSION

With an extraordinarily low density, WASP-107b motivated both an extensive radial-velocity follow-up program and a detailed study of the physics governing the accretion of its gas envelope. As a first step, we use a 4-year *Keck*/HIRES survey to provide a more precise measurement of WASP-107b’s mass ( $M_b = 30.5 \pm 1.7 M_\oplus$ ), 20% (or  $2.2\sigma$ ) lower than the  $38 \pm 3 M_\oplus$  based on the CORALIE data published in the discovery paper (Anderson et al. 2017). The newly inferred mass indicates

an extremely large envelope mass fraction of  $> 85\%$  for solar-metallicity gas. The corresponding core mass is  $< 4.6 M_{\oplus}$  at  $3\sigma$ , substantially lower than traditionally assumed to be necessary to trigger the accretion of a massive gas envelope. Higher core masses would only be possible if the planet’s atmosphere had an enhanced metallicity, which we constrain to less than 12.5 times the solar value by mass at  $3\sigma$  using interior structure models.

WASP-107b might be one of the planets that came the closest to experiencing the full extent of runaway gas accretion without becoming a gas giant. While runaway accretion was likely launched at  $\gtrsim 1$  AU, the envelope growth of this super-puffy Neptune was probably stunted as a result of its migration to the inner disk. This scenario could also explain the formation of the super-puff Kepler-90g found at 0.7 AU (Liang et al. 2020). In-situ formation, on the other hand, is ruled out for such a high gas-to-core mass ratio as it would require higher metallicities than allowed by the large radius of this planet.

We note that the orbital constraints of WASP-107b are consistent with a moderate eccentricity ( $e_b = 0.06 \pm 0.04$ ). If confirmed, a non-zero eccentricity could point towards recent dynamical interactions or provide an alternative explanation for its large radius via tidal inflation, provided the tidal quality factor of WASP-107b is  $\lesssim 10^5$ . The study of this planet thus holds the potential to inform the role that inflation plays in the observed diversity in the bulk densities of exo-Neptunes.

Our updated planetary mass, which affects the estimated surface gravity, motivates a complete re-analysis of all the published transmission spectroscopy data of WASP-107b. We are thus conducting a joint retrieval analysis of all the existing transit and eclipse spectroscopic observations, which we will present in an upcoming paper (Piaulet et al., in prep.). Our improved understanding of the system and the bulk properties of WASP-107b will also be essential for the interpretation of JWST Guaranteed Time Observations (4 transits and 1 eclipse observation) and GO programs.

We furthermore detect a long-period more massive companion to this close-in planet on a highly eccentric orbit ( $e_c = 0.28 \pm 0.07$ ) which may have influenced the migration and orbital obliquity of WASP-107b. We find that the sky-projected angular separation of planet c is of only  $26_{-5}^{+8}$  mas using the posterior distributions on the period, eccentricity and argument of periastron resulting from our RV fit and assuming a random inclination of WASP-107c’s orbit. This planet is thus too close to its host to be detectable via direct imaging with current instrumentation. In terms of its astrometric detectabil-

ity, the reflex motion of WASP-107 as the planet travels around its orbit results in an astrometric signature of  $\approx 10 - 30 \mu\text{as}$ , smaller than the *Gaia* DR2 RA/DEC uncertainty of  $44 \mu\text{as}$  (Gaia Collaboration et al. 2018). This suggests that WASP-107c could hardly be detected using the DR2 results but might be detectable in the future using the 5-year *Gaia* time-series (Rubenzahl et al., submitted).

Looking ahead, the inferred lower mass and density of WASP-107b make it a key planet to understand and reexamine how massive a planetary core needs to be in order to accrete substantial amounts of gas.

We thank the anonymous reviewer, whose comments greatly improved the paper. C.P. wishes to thank D. Lai and M. al-Dib for useful discussions regarding the formation and orbital dynamics of this unique system, as well as S. Pelletier, P. Gupta, J. Chan, L.-P. Coulombe, P.-A. Roy, S. Delisle and M. Papillon for useful comments on the first manuscript of this paper. We thank D. Anderson for providing us the CORALIE RVs of WASP-107.

C.P. is supported by the Technologies for Exoplanetary Science (TEPS) CREATE program. C.P. and B.B. acknowledge financial support by the Fonds de Recherche Québécois—Nature et Technologie (FRQNT; Québec). B.B. further acknowledges financial support by the Natural Sciences and Engineering Research Council (NSERC) of Canada. R. A. R. is supported by the National Science Foundation Graduate Research Fellowship Program under Grant No. DGE-1745301. Any opinions, findings, and conclusions or recommendations expressed in this material are those of the author(s) and do not necessarily reflect the views of the National Science Foundation. A.W.H. acknowledges support from the K2 Guest Observer Program and NASA’s Key Strategic Mission Support program.

This research was enabled in part by support provided by Calcul Québec (<https://www.calculquebec.ca/>), Compute Canada ([www.computeCanada.ca](http://www.computeCanada.ca)), and the Savio computational cluster resource provided by the Berkeley Research Computing program at the University of California, Berkeley (supported by the UC Berkeley Chancellor, Vice Chancellor for Research, and Chief Information Officer).

This work has made use of data from the European Space Agency (ESA) mission *Gaia* (<https://www.cosmos.esa.int/gaia>), processed by the *Gaia* Data Processing and Analysis Consortium (DPAC, <https://www.cosmos.esa.int/web/gaia/dpac/consortium>). Funding for the DPAC has been provided by national institu-

tions, in particular the institutions participating in the Gaia Multilateral Agreement.

This research has made use of NASA’s Astrophysics Data System and the NASA Exoplanet Archive, which is operated by the California Institute of Technology, under contract with the National Aeronautics and Space Administration under the Exoplanet Exploration Program.

This work was based on observations obtained at the W. M. Keck Observatory, which is operated jointly by the University of California and the California Institute of Technology.

The authors wish to recognize and acknowledge the very significant cultural role and reverence that the sum-

mit of Maunakea has always had within the indigenous Hawaiian community. We are most fortunate to have the opportunity to conduct observations from this mountain.

*Software:* Astropy (Astropy Collaboration et al. 2013), bayev (<https://github.com/exord/bayev>), corner (Foreman-Mackey 2016), emcee (Foreman-Mackey et al. 2013), isoclassify (Huber et al. 2017b), Matplotlib (Hunter 2007), Numpy/Scipy (van der Walt et al. 2011), RadVel (Fulton et al. 2018), smint (<https://github.com/cpiaulet/smint>), SpecMatch-emp (Yee et al. 2017)

## REFERENCES

- Agüeros, M. A., Bowsher, E. C., Bochanski, J. J., et al. 2018, *ApJ*, 862, 33
- Alexander, R., Pascucci, I., Andrews, S., et al. 2014, *Protostars and Planets VI*, 475
- Allart, R., Bourrier, V., Lovis, C., et al. 2019, *A&A*, 623, A58
- Anderson, D. R., Collier Cameron, A., Delrez, L., et al. 2017, *A&A*, 604, A110
- Angus, R., Beane, A., Price-Whelan, A. M., et al. 2020, *AJ*, 160, 90
- Astropy Collaboration, Robitaille, T. P., Tollerud, E. J., et al. 2013, *A&A*, 558, A33
- Bailer-Jones, C. A. L., Rybizki, J., Foesneau, M., et al. 2018, *AJ*, 156, 58
- Batalha, N. E., Lewis, T., Fortney, J. J., et al. 2019, *ApJL*, 885, L25
- Batygin, K. & Adams, F. C. 2013, *ApJ*, 778, 169
- Benneke, B., Knutson, H. A., Lothringer, J., et al. 2019, *Nature Astronomy*, 377
- Brahm, R., Espinoza, N., Rabus, M., et al. 2019, *MNRAS*, 483, 1970
- Butler, R. P., Marcy, G. W., Williams, E., et al. 1996, *PASP*, 108, 500
- Chabrier, G., Mazevet, S., & Soubiran, F. 2019, *The Astrophysical Journal*, 872, 51
- Cloutier, R., Astudillo-Defru, N., Doyon, R., et al. 2019, *A&A*, 621, A49
- Curtis, J. L., Agüeros, M. A., Douglas, S. T., et al. 2019, *ApJ*, 879, 49
- Curtis, J., Agüeros, M., & Douglas, S. 2020, *American Astronomical Society Meeting Abstracts*
- Curtis, J. L., Agüeros, M. A., Matt, S. P., et al. 2020, *arXiv:2010.02272*
- Cutri, R. M., Skrutskie, M. F., van Dyk, S., et al. 2003, *VizieR Online Data Catalog*, II/246
- Dai, F., & Winn, J. N. 2017, *AJ*, 153, 205
- Dawson, R. I., & Johnson, J. A. 2018, *ARA&A*, 56, 175
- Foreman-Mackey, D., Hogg, D. W., Lang, D., et al. 2013, *Publications of the Astronomical Society of the Pacific*, 125, 306
- Foreman-Mackey, D. 2016, *The Journal of Open Source Software*, 1, 24. doi:10.21105/joss.00024
- Fortney, J. J., Marley, M. S., & Barnes, J. W. 2007, *ApJ*, 659, 1661
- Fulton, B. J., Petigura, E. A., Blunt, S., et al. 2018, *PASP*, 130, 44504
- Gaia Collaboration, Brown, A. G. A., Vallenari, A., et al. 2018, *A&A*, 616, A1
- Ginzburg, S., Schlichting, H. E., & Sari, R. 2016, *ApJ*, 825, 29
- Ginzburg, S., Schlichting, H. E., & Sari, R. 2018, *MNRAS*, 476, 759
- Goldreich, P., & Soter, S. 1966, *Icarus*, 5, 375
- Guillot, T. 2005, *Annual Review of Earth and Planetary Sciences*, 33, 493
- Gupta, A. & Schlichting, H. E. 2020, *MNRAS*, 493, 792. doi:10.1093/mnras/staa315
- Haisch, K. E., Lada, E. A., & Lada, C. J. 2001, *ApJ*, 553, L153
- Hartmann, L., Calvet, N., Gullbring, E., & D’Alessio, P., *ApJ*, 495, 385
- Høg, E., Fabricius, C., Makarov, V. V., et al. 2000, *A&A*, 355, L27
- Howard, A. W., Johnson, J. A., Marcy, G. W., et al. 2010, *ApJ*, 721, 1467
- Huber, K. F., Czesla, S., & Schmitt, J. H. M. M. 2017, *A&A*, 597, A113

- Huber, D., Zinn, J., Bojsen-Hansen, M., et al. 2017, *ApJ*, 844, 102
- Hunter, J. D. 2007, *Computing in Science and Engineering*, 9, 90
- Jackson, B., Barnes, R., & Greenberg, R. 2009, *ApJ*, 698, 1357
- Kiseleva, L. G., Eggleton, P. P., & Mikkola, S. 1998, *MNRAS*, 300, 292
- Kreidberg, L., Line, M. R., Thorngren, D., et al. 2018, *ApJ*, 858, L6
- Lai, D. 2014, *MNRAS*, 440, 3532
- Lainey, V., Arlot, J.-E., Karatekin, Ö., et al. 2009, *Nature*, 459, 957
- Lambrechts, M., & Lega, E. 2017 *A&A*, 606, A146
- Lee, E. J., Chiang, E., & Ormel, C. W., *ApJ*, 797, 95
- Lee, E. J., & Chiang, E. 2015, *ApJ*, 811, 41
- Lee, E. J., & Chiang, E. 2016, *ApJ*, 817, 90
- Lee, E. J. 2019, *ApJ*, 878, 36
- Liang, Y., Robnik, J., & Seljak, U. 2020, arXiv:2011.08515
- Lin, D. N. C., Bodenheimer, P., & Richardson, D. C. 1996, *Nature*, 380, 606
- Lopez, E. D., & Fortney, J. J. 2014, *ApJ*, 792, 1
- Lynden-Bell, D. & Pringle, J. E. 1974, *MNRAS* 168, 603
- Mamajek, E. E. 2009, *American Institute of Physics Conference Series*, 3
- Mazeh, T., Holczer, T., & Faigler, S. 2016, *A&A*, 589, A75
- Maxted, P. F. L., Serenelli, A. M., & Southworth, J. 2015, *A&A*, 575, A36
- Millholland, S., Petigura, E., & Batygin, K. 2020, *ApJ*, 897, 7. doi:10.3847/1538-4357/ab959c
- Mizuno, H. 1980, *Progress of Theoretical Physics*, 64, 544
- Močnik, T., Hellier, C., Anderson, D. R., et al. 2017, *MNRAS*, 469, 1622
- Mordasini, C. 2014, *A&A*, 572, A118
- Nagasawa, M., Ida, S., & Bessho, T. 2008, *ApJ*, 678, 498
- Nelson, B. E., Ford, E. B., Buchner, J., et al. 2020, *AJ*, 159, 73
- Owen, J. E., Ercolano, B., & Clarke, C. J. 2011, *MNRAS*, 412, 13
- Owen, J. E., & Wu, Y. 2013, *ApJ*, 775, 105
- Owen, J. E., & Wu, Y. 2016, *ApJ*, 817, 107
- Owen, J. E., & Wu, Y. 2017, *ApJ*, 847, 29
- Owen, J. E., & Lai, D. 2018, *MNRAS*, 479, 5012
- Ormel, C. W. 2014, *ApJL*, 789, L18
- Papaloizou, J. C. B., Nelson, R. P., Kley, W., et al. 2007, *Protostars and Planets V*, 655
- Penev, K., Bouma, L. G., Winn, J. N., et al. 2018, *AJ*, 155, 165
- Pepper, J., Rodriguez, J. E., Collins, K. A., et al. 2017, *AJ*, 153, 215
- Perrakis, K., Ntzooufras, I., & Tsionas, E. G. 2014, *Comput. Stat. Data Anal.* 77, 54
- Perri, F., & Cameron, A. G. W. 1974, *Icarus*, 22, 416
- Petigura, E. A., Sinukoff, E., Lopez, E. D., et al. 2017, *AJ*, 153, 142
- Petrovich, C., Muñoz, D. J., Kratter, K. M., et al. 2020, arXiv:2008.08587
- Pfalzner, S., Steinhausen, M., & Menten, K. 2014, *ApJ*, 793, L3
- Piso, A.-M. A., Youdin, A. N., & Murray-Clay, R. A. 2015, *ApJ*, 800, 82
- Podolak, M., & Marley, M. S. 1991, *BAAS* 23, 1164
- Pollack, J. B., Hubickyj, O., Bodenheimer, P., et al. 1996, *Icarus*, 124, 62
- Shen, Y., & Turner, E. L. 2008, *ApJ*, 685, 553
- Spake, J. J., Sing, D. K., Evans, T. M., et al. 2018, *Nature*, 557, 68
- Tanigawa, T., & Tanaka, H. 2016, *ApJ*, 823, 48
- Thorngren, D. P., Fortney, J. J., Murray-Clay, R. A., et al. 2016, *ApJ*, 831, 64
- Thorngren, D., & Fortney, J. J. 2019, *The Astrophysical Journal*, 874, L31
- , ANEOS–Analytic Equations of State for Shock Physics Codes, Sandia Natl. Lab. Doc. SAND89-2951
- Trotta, R. 2008, *Contemporary Physics*, 49, 71
- van der Walt, S., Colbert, S. C., & Varoquaux, G. 2011, *Computing in Science and Engineering*, 13, 22
- Vogt, S. S., Allen, S. L., Bigelow, B. C., et al. 1994, *Instrumentation in Astronomy VIII*, 362
- Yee, S. W., Petigura, E. A., & von Braun, K. 2017, *ApJ*, 836, 77
- Yee, S. W., Petigura, E. A., Fulton, B. J., et al. 2018, *AJ*, 155, 255
- Zanazzi, J. J., & Lai, D. 2018, *MNRAS*, 478, 835